© 2015. Published by The Company of Biologists Ltd | Development (2015) 142, 118-127 doi:10.1242/dev.114843

RESEARCH ARTICLE

Chd1 is essential for the high transcriptional output and rapid growth of the mouse epiblast

Marcela Guzman-Ayala[1,2,‡,¶], Michael Sachs[1,2,¶,§], Fong Ming Koh[1,2], Courtney Onodera[1,3,4], Aydan Bulut-Karslioglu[1,2], Chih-Jen Lin[1,2], Priscilla Wong[1,2], Rachel Nitta[1,2], Jun S. Song[1,3,4,*] and Miguel Ramalho-Santos[1,2,]**

ABSTRACT

The pluripotent mammalian epiblast undergoes unusually fast cell proliferation. This rapid growth is expected to generate a high transcriptional demand, but the underlying mechanisms remain unknown. We show here that the chromatin remodeler Chd1 is required for transcriptional output and development of the mouse epiblast. *Chd1*$^{-/-}$ embryos exhibit proliferation defects and increased apoptosis, are smaller than controls by E5.5 and fail to grow, to become patterned or to gastrulate. Removal of p53 allows progression of *Chd1*$^{-/-}$ mutants only to E7.0-8.0, highlighting the crucial requirement for Chd1 during early post-implantation development. *Chd1*$^{-/-}$ embryonic stem cells (ESCs) have a self-renewal defect and a genome-wide reduction in transcriptional output at both known mRNAs and intergenic transcripts. These transcriptional defects were only uncovered when cell number-normalized approaches were used, and correlate with a lower engagement of RNAP II with transcribed genes in *Chd1*$^{-/-}$ ESCs. We further show that Chd1 directly binds to ribosomal DNA, and that both *Chd1*$^{-/-}$ epiblast cells *in vivo* and ESCs *in vitro* express significantly lower levels of ribosomal RNA. In agreement with these findings, mutant cells *in vivo* and *in vitro* exhibit smaller and more elongated nucleoli. Thus, the RNA output by both Pol I and II is reduced in *Chd1*$^{-/-}$ cells. Our data indicate that Chd1 promotes a globally elevated transcriptional output required to sustain the distinctly rapid growth of the mouse epiblast.

KEY WORDS: Chromatin, Epiblast proliferation, Epigenetics, Pluripotency, Transcription

INTRODUCTION

Embryonic development involves a sophisticated coordination of cell proliferation and differentiation. Mammalian embryos display the fastest cell proliferation rate in the pluripotent epiblast soon after implantation, with doubling times of 2-8 h at embryonic day (E) 5.5-6.5 (Snow, 1977). This growth is essential to establish the cell population that will undergo gastrulation and give rise to the embryo proper (Lewis and Rossant, 1982; Power and Tam, 1993; Snow, 1977). Unlike the early embryos of other model organisms, such as *Drosophila* or *Xenopus*, the mammalian post-implantation epiblast has minimal maternal supplies of mRNA and/or protein left over from the zygote stage. Therefore, the fast proliferation and growth of the epiblast may generate a high demand for transcriptional output by the RNA polymerases (RNAPs) and for ribosome biogenesis. However, how the transcriptional output of rapidly expanding pluripotent cells is regulated remains unknown.

Pluripotent cells have a decondensed chromatin organization that is associated with genome-wide elevated levels of transcription, including at intergenic regions (Ahmed et al., 2010; Efroni et al., 2008; Meshorer and Misteli, 2006). Moreover, embryonic stem cells (ESCs) have higher levels of the activating histone mark H3K4me3 than differentiated cells, and Wdr5, a core component of the Trithorax complexes responsible for trimethylation of H3K4, is essential for ESC self-renewal (Ang et al., 2011). Chromatin factors that act as readers of activating histone marks, such as H3K4me3, might therefore be important regulators of the transcriptional output of pluripotent cells.

Chromodomain helicase DNA-binding protein 1 (Chd1) is a conserved protein associated with decondensed chromatin and transcription in several species (Sims et al., 2005; Stokes et al., 1996; Woodage et al., 1997). Chd1 binds with high specificity to H3K4me2/3 (Flanagan et al., 2005; Sims et al., 2007) and enhances the transcriptional activity of RNAP II on a synthetic chromatin template (Lin et al., 2011). Chd1 has recently been shown to remove the barrier of promoter-proximal nucleosomes and facilitate release of RNAP II into productive elongation (Skene et al., 2014). Mouse embryonic fibroblasts expressing a dominant negative form of Chd1 have reduced turnover of promoter-proximal nucleosomes and lower levels of RNAP II S2p, a mark of transcriptional elongation, at essentially all expressed genes (Skene et al., 2014). In face of these insights into the biochemical mode of action of Chd1 at transcribed genes, it remains unclear whether Chd1 has any role in the cell transcriptome, because yeast *Chd1* mutants (Gkikopoulos et al., 2011) and *Chd1* RNAi mouse ESCs (Gaspar-Maia et al., 2009) have very minimal changes to their transcriptional profile, as assessed using standard microarray methods.

We previously reported that Chd1 binding in the ESC genome is highly correlated with H3K4me3 and RNAP II, and that *Chd1* RNAi ESCs can be expanded in the undifferentiated state but show self-renewal defects and a propensity to accumulate heterochromatin (Gaspar-Maia et al., 2009). These findings raise the question of which role Chd1 might play in pluripotent cells in the context of the developing embryo. Studies in other organisms argue against an essential role for Chd1: yeast *Chd1* mutants are viable (Tsukiyama et al., 1999; Woodage et al., 1997), and *Drosophila Chd1* mutants are

[1]Eli and Edythe Broad Center of Regeneration Medicine and Stem Cell Research, 35 Medical Center Way, University of California, San Francisco, CA 94143, USA. [2]Center for Reproductive Sciences, Department of Obstetrics, Gynecology and Reproductive Sciences, 35 Medical Center Way, University of California, San Francisco, CA 94143, USA. [3]Institute for Human Genetics, 35 Medical Center Way, University of California, San Francisco, CA 94143, USA. [4]Department of Epidemiology and Biostatistics, 35 Medical Center Way, University of California, San Francisco, CA 94143, USA.
*Present address: Departments of Bioengineering and Physics, University of Illinois, Urbana-Champaign, Urbana, IL 61801, USA. ‡Present address: Flexus Biosciences, 75 Shoreway Road, Suite D, San Carlos, CA 94070, USA.
§Present address: Genentech, 1 DNA Way, South San Francisco, California 94080, USA.
¶These authors contributed equally to this work

**Author for correspondence (miguel.ramalho-santos@ucsf.edu)

Received 7 July 2014; Accepted 3 November 2014

Development (2015) 142, 118-127 doi:10.1242/dev.114843

also viable, although they have wing abnormalities and are infertile (Konev et al., 2007; McDaniel et al., 2008). Morpholino-mediated knockdown of the gene amplified in liver cancer (*ALC1*), also known as *Chd1l*, in early mouse embryos prevents development to the blastocyst stage (Snider et al., 2013). However, the name *Chd1l* might be confusing, because *ALC1*/*Chd1l* is only distantly related to *Chd1* (or indeed to other Chd family members): *ALC1*/*Chd1l* lacks the H3K4me3-binding chromo-domains and the DNA-binding domain of *Chd1*, and instead has a macro-domain (Flaus et al., 2006).

Here, we report that genetic deletion of mouse *Chd1* results in arrest of epiblast development at E5.5-6.5, prior to the onset of gastrulation. We further show that Chd1 is required for the maintenance of optimal transcriptional output by RNAP I and II in ES and epiblast cells. These results indicate that Chd1 promotes a globally elevated transcriptional output that underlies the rapid growth of the pluripotent epiblast.

RESULTS

Mouse Chd1 is required in the epiblast for post-implantation development

To understand the role of mammalian Chd1 *in vivo*, we generated mice and ESCs carrying either null or conditional (floxed) alleles of *Chd1* (supplementary material Fig. S1A). The *Chd1* null allele lacks exon 16, which codes for a conserved fragment of the helicase domain. The null allele also includes an IRES-*lacZ* construct to report on endogenous Chd1 expression (supplementary material Fig. S1A). Cre-mediated recombination of the conditional allele produces the same exon 16 deletion and frame-shift. Both approaches to delete Chd1 were validated by Southern blotting, western blotting and qRT-PCR (supplementary material Fig. S1B,C, Fig. S7A). Whereas Chd1 heterozygous ($Chd1^{+/-}$) mice are healthy, fertile and appear phenotypically normal, no Chd1 homozygous ($Chd1^{-/-}$) pups are recovered from heterozygous intercrosses, indicating that Chd1 is essential for embryonic development (Table 1). Embryos from heterozygous intercrosses are observed at close to Mendelian ratios at E9.5, but by this stage, all $Chd1^{-/-}$ embryos are very small and undergo resorption (Fig. 1A). This phenotype is consistently observed in both inbred (129) and mixed (129/BL6) backgrounds. The presence of resorbed embryos suggests that *Chd1* mutants survive earlier stages of development and arrest following implantation. In agreement with this notion, $Chd1^{-/-}$ embryos form morphologically normal blastocysts at E3.5, and ESCs can be derived from them at normal Mendelian distributions (Table 1, Fig. 1C, and see below).

Developmental defects at peri-implantation can be due to abnormalities in the embryo proper, extra-embryonic tissues or in both. We therefore aimed to test whether Chd1 is required for development of the embryo proper. Chd1 is expressed maternally and throughout pre-implantation development (supplementary material Fig. S2). We were not able to perform immunofluorescence (IF) for Chd1 in post-implantation embryos using available commercial antibodies, but the $Chd1^{lacZ}$ reporter allele is preferentially expressed in the E6.5 epiblast (Fig. 1D). We carried out deletion of *Chd1* specifically in the epiblast using the conditional allele and the Sox2-Cre deleter strain (Hayashi et al., 2002). Epiblast-specific deletion of *Chd1* results in an embryo resorption phenotype by E9.5 that is very similar to that of the full *Chd1* mutants (Fig. 1B). These data do not exclude a potential additional role for Chd1 in the extra-embryonic tissues, but document that Chd1 is required in the post-implantation epiblast for its subsequent development.

Table 1. Intercrosses of $Chd1^{+/-}$ mice produce E3.5 and E6.5 embryos at the expected Mendelian distribution, but no $Chd1^{-/-}$ pups are observed at birth

	Total *n*	$Chd1^{+/+}$	$Chd1^{+/-}$	$Chd1^{-/-}$
E3.5 (ES cells)	40 (7 litters)	10 (25%)	21 (52.5%)	9 (22.5%)
E6.5	244 (28 litters)	70 (28.7%)	123 (50.4%)	42+9* (20.9%)
At birth	51 (8 litters)	19 (37%)	32 (63%)	0

(*) Nine very small embryos collected at E6.5 could not be genotyped and were presumed to be $Chd1^{-/-}$.

$Chd1^{-/-}$ embryos do not sustain epiblast gene expression, establish the anterior-posterior (A/P) axis or gastrulate

In order to better define the developmental phenotype of $Chd1^{-/-}$ embryos, we next analyzed the expression of *Oct4* (also known as *Pou5f1*), *Nodal* and *Fgf5*. These genes are specifically expressed throughout the epiblast at E5.5 (Hébert et al., 1991; Mesnard et al., 2006; Rosner et al., 1990) and are important markers of pluripotency. We observed that *Oct4*, *Nodal* and *Fgf5* are expressed in the $Chd1^{-/-}$ epiblast at E5.5 (Fig. 2A). However, by E6.5, the mutant epiblast expresses greatly reduced levels of *Oct4* and *Fgf5* relative to littermate controls (Fig. 2B). These data indicate that Chd1 is not required for induction of the epiblast cell fate, but rather

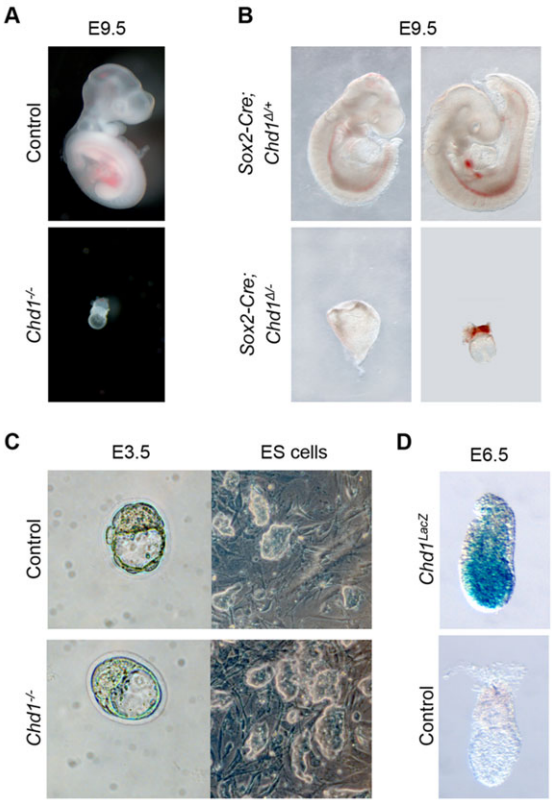

Fig. 1. Chd1 is required for development of the post-implantation mouse epiblast. (A) $Chd1^{-/-}$ embryos recovered at E9.5 are in the process of being resorbed. (B) Epiblast-specific deletion of *Chd1* (*Sox2-Cre;*$Chd1^{\Delta/-}$) phenocopies the $Chd1^{-/-}$ phenotype and leads to resorption at E9.5 when compared with littermate controls (*Sox2-Cre;*$Chd1^{\Delta/+}$). (C) There is no obvious morphological difference between control and $Chd1^{-/-}$ blastocysts at E3.5, and $Chd1^{-/-}$ ESCs can be derived. (D) The $Chd1^{lacZ}$ reporter allele is preferentially expressed in the epiblast at E6.5 (top); control embryos (bottom) not carrying the reporter allele show no signal when stained with X-gal. All images for each panel were taken at the same magnification.

Development (2015) 142, 118-127 doi:10.1242/dev.114843

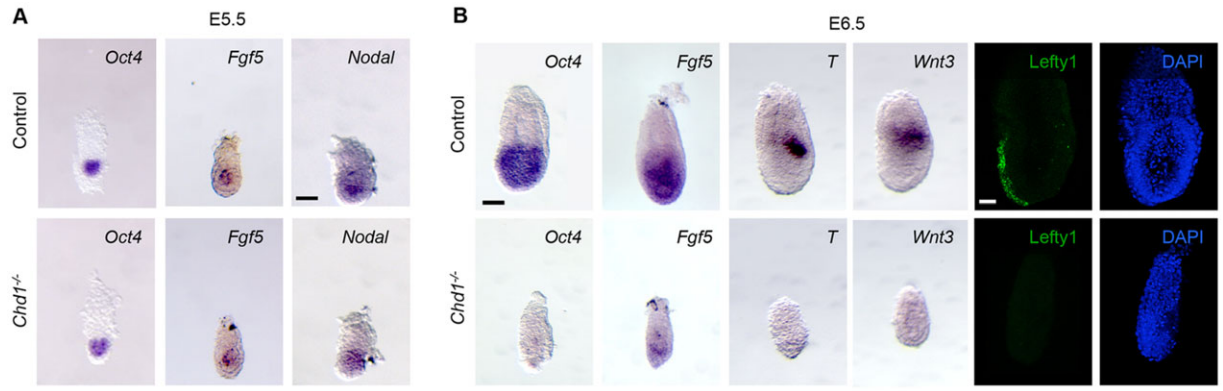

Fig. 2. The epiblast forms but is not maintained in *Chd1*$^{-/-}$ embryos. (A) At E5.5, mRNAs of the epiblast markers *Oct4*, *Nodal* and *Fgf5* are expressed normally in control (top) and *Chd1*$^{-/-}$ embryos (bottom) (*Oct4*, *n*=4; *Nodal*, *n*=4; *Fgf5*, *n*=3). (B) At E6.5, *Chd1*$^{-/-}$ embryos (bottom) are smaller than controls (top) and have reduced expression of *Oct4* (*n*=6) and *Fgf5* mRNA (*n*=7). Mutant embryos also fail to establish A/P patterning of the epiblast: *Chd1*$^{-/-}$ embryos do not induce expression of posterior/primitive streak mRNAs *T* (*n*=2) nor *Wnt3* (*n*=3), and do not express the AVE protein marker Lefty1 (*n*=7). In control embryos, anterior is to the left and posterior to the right. All WISH images were taken at the same magnification. Scale bars: 50 µm.

for its maintenance. This is reinforced by analysis of gene expression during differentiation of embryoid bodies (EBs) *in vitro*. We observed that *Chd1*$^{-/-}$ cells are capable of robustly inducing markers of all three germ layers upon differentiation (supplementary material Fig. S3A).

We found that, by E6.5, *Chd1*$^{-/-}$ embryos are highly reduced in size compared with controls (Fig. 2). Moreover, expression of *Lefty1*, a marker of the anterior visceral endoderm (AVE) and a regulator of future anterior structures (Perea-Gomez et al., 2002), is absent in the mutants (Fig. 2B). In addition, the mutants are unable to undergo gastrulation, as highlighted by the lack of expression of the nascent mesoderm markers *brachyury* (*T*) and *Wnt3* (Liu et al., 1999) at the posterior end of the embryo (Fig. 2B). The expression of markers of the extra-embryonic ectoderm, such as *Cdx2* and *Bmp4*, is also absent at E6.5 in *Chd1*$^{-/-}$ embryos (supplementary material Fig. S4), probably due to the reciprocal molecular interactions between the epiblast and the extraembryonic ectoderm that occur at the onset of gastrulation (Guzman-Ayala et al., 2004). Thus, *Chd1*$^{-/-}$ embryos arrest in the transition between E5.5 and E6.5, prior to anterior-posterior (A/P) patterning and initiation of gastrulation.

The E5.5 *Chd1*$^{-/-}$ epiblast does not grow due to increased apoptosis and defective cell cycle

A minimum number of cells are thought to be required for the epiblast to undergo patterning and gastrulation (Lewis and Rossant, 1982; Power and Tam, 1993). Notably, the number of epiblast cells is already significantly reduced in the mutants by E5.5 (Fig. 3A), that is, prior to detectable differences in the expression of epiblast markers (Fig. 2). These data are supported by cell counts *in vitro*: *Chd1*$^{-/-}$ ESCs, although viable, display a self-renewal deficit both in colony formation assays and in bulk expansion, in agreement with our previous findings using RNAi (Gaspar-Maia et al., 2009) (supplementary material Fig. S3B,C; and data not shown).

A reduction in epiblast cell number could be due to increased apoptosis and/or a defective or delayed cell cycle, and we found evidence for both in *Chd1*$^{-/-}$ embryos. Control E5.5 embryos are essentially devoid of apoptotic cells marked by cleaved Parp (no cleaved Parp cells in 16/20 embryos and 1 or 2 cleaved Parp cells in 4/20 embryos, see Fig. 3B), in agreement with recently reported findings (Bedzhov and Zernicka-Goetz, 2014). By contrast, cleaved Parp is consistently detected in E5.5 *Chd1*$^{-/-}$ embryos (more than five cleaved Parp cells in 7/7 embryos). To analyze the cell cycle state of the mutant epiblast, we assayed E5.5 embryos for 5-Ethynyl-2′-deoxyuridine (EdU) incorporation (S phase) and phospho-Histone 3 staining (pH3, M phase). Labeled epiblast cells were counted and presented as a percentage of the epiblast cell number, referred to as the S phase index for EdU or mitotic index for pH3. We found no statistically significant difference in the S phase index between mutant and control epiblasts (Fig. 3C). Interestingly, the mitotic index in the *Chd1*$^{-/-}$ epiblast was about 40% higher than in controls (Fig. 3D). This accumulation in mitosis without changes in the proportion of cells in S phase suggests that mutant cells undergo a delay in the completion of mitosis. Alternatively, the increased mitotic index in the mutants could simply be due to a developmental delay. In this case, we would expect earlier stage embryos to have higher mitotic indices. However, we did not observe any correlation between mitotic index and the size of the epiblast (defined by the number of cells) in control embryos (Fig. 3E).

To independently explore the potential mitotic defects of *Chd1*$^{-/-}$ embryos, we quantified the number of foci of H3 variant CENP-A (Cenpa – Mouse Genome Informatics) in each epiblast cell. Proper incorporation of CENP-A at centromeric regions is considered indicative of a successful mitotic exit (Jansen et al., 2007). Chd1 depletion has been previously reported to lead to reduced CENP-A incorporation in cultured avian cells (Okada et al., 2009). In agreement, we found that the number of CENP-A foci in the *Chd1*$^{-/-}$ epiblast was significantly reduced (Fig. 3F). Taken together, these data indicate that the smaller *Chd1*$^{-/-}$ epiblast at E5.5 is due to an increase in apoptotic cell death and a delay in progression through mitosis.

Several mutations in essential growth or DNA repair genes that lead to peri-implantation lethality similar to the case of *Chd1*$^{-/-}$ embryos can be rescued to mid-gestation (~E9.5-12.5) upon removal of p53. Therefore, we explored the development of *Chd1*$^{-/-}$ embryos in a *p53*$^{-/-}$ background. Surprisingly, we found that removal of p53 from the *Chd1* mutant background only allows development to ~E7.0-8.0. When recovered at E8.5, *Chd1*$^{-/-}$*;p53*$^{-/-}$ embryos are severely delayed and arrested (Fig. S5). Thus, Chd1 is critically required for post-implantation development, even in the absence of p53.

Chd1$^{-/-}$ ESCs have lower transcriptional output per cell

In order to better understand the mechanism of action of Chd1 in pluripotent cells, we generated *ROSA26CreER;Chd1*$^{fl/-}$ ESCs, in which *Chd1* deletion can be induced by exposure to tamoxifen.

Development (2015) 142, 118-127 doi:10.1242/dev.114843

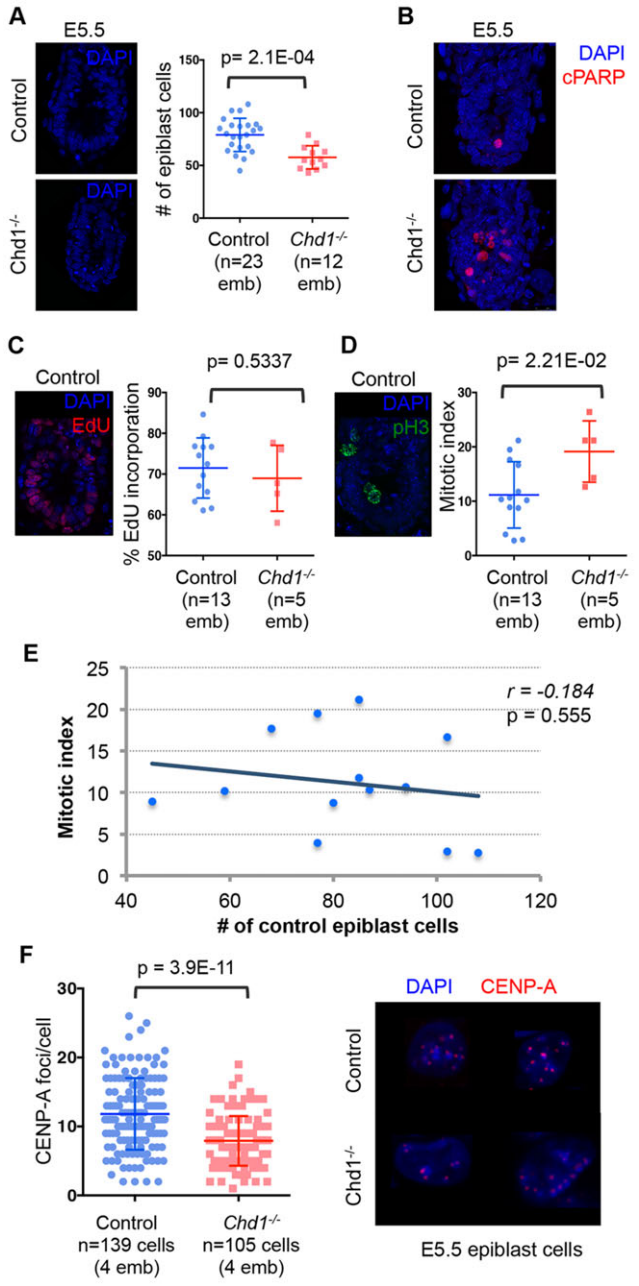

Fig. 3. The *Chd1*$^{-/-}$ epiblast does not grow due to defective cell cycle and increased apoptosis. (A) The number of cells of the E5.5 epiblast is significantly reduced in *Chd1*$^{-/-}$ embryos compared with control embryos. (B) Representative embryos stained for cParp showing that apoptotic cells are consistently detected in *Chd1*$^{-/-}$ embryos (7/7), but are rarely observed (1-2 cells in 4/20 embryos) or not at all (0 cells in 16/20 embryos) in controls. Images represent a projection of five different confocal planes through the embryo. (C) *Chd1*$^{-/-}$ embryos show no significant difference in proportion of cells incorporating EdU in the epiblast compared with controls at E5.5. (D) The mitotic index, calculated as the percentage of epiblast cells stained with pH3, is significantly higher in the *Chd1*$^{-/-}$ epiblast (19.15 ±5.631) compared with the control epiblast (11.17±6.095) at E5.5. (E) There is no correlation between mitotic index and number of epiblast cells in control embryos, suggesting that the increased mitotic index of the mutants is not due to a developmental delay. (F) The number of CENP-A foci detected per epiblast cell is significantly reduced in mutants (7.914± 3.601) compared with controls (11.82±5.197) at E5.5. All results are mean±s.d. In all cases, a single *z*-stack from one representative embryo with DAPI staining and IF for the indicated marker is shown, with the exception of panel B, in which a full projection is shown.

In view of the role of Chd1 in facilitating RNAP II release into productive elongation (Skene et al., 2014) and the self-renewal deficit of Chd1-deficient ESCs (supplementary material Fig. S3; and data not shown), we reasoned that distinct transcriptional changes might be evident in *Chd1*$^{-/-}$ ESCs. Additionally, in line with previous observations in *Chd1* RNAi ESCs (Gaspar-Maia et al., 2009), *Chd1*$^{-/-}$ cells exhibit a global accumulation of Hp1a (Cbx5 – Mouse Genome Informatics), suggestive of an increase in heterochromatin (supplementary material Fig. S6). However, similar to Chd1-null strains of *Saccharomyces cerevisiae* and *Schizosaccharomyces pombe* (Hennig et al., 2012; Pointner et al., 2012), initial microarray analyses showed very few genes changing in expression in *Chd1*$^{-/-}$ ESCs (data not shown). Although we had previously reported that *Chd1* RNAi ESCs upregulated genes of the neural lineage (Gaspar-Maia et al., 2009), we subsequently found that this could be suppressed by high doses of commercially available leukemia inhibitory factor (LIF) (data not shown), the conditions we currently use (see Materials and Methods). Thus, *Chd1*$^{-/-}$ ESCs appeared to have a largely unchanged relative distribution of expression levels across genes. However, we considered the possibility that Chd1 might globally regulate absolute transcription levels, given its ubiquitous, genome-wide association with RNAP II (Gaspar-Maia et al., 2009). Standard techniques used to measure relative changes in gene expression, such as qRT-PCR, microarrays or RNA-seq, rely on normalization for RNA amount and cannot detect a global shift in expression, as has been recently described for the case of cMyc overexpression (Lin et al., 2012; Lovén et al., 2012; Nie et al., 2012). In order to overcome this obstacle, we performed cell number-normalized RNA-seq by isolating identical numbers of two pairs of control and mutant ESCs and adding a set of spike-in RNAs for downstream normalization (see Materials and Methods). Remarkably, this analysis revealed that the transcriptional output of *Chd1*$^{-/-}$ ESCs is significantly reduced genome-wide relative to control ESCs (Fig. 4A,B), with a median reduction of 24% across all genes (Fig. 4C, Wilcoxon $P<2.2E-16$). Whereas these data are considerably more variable for intergenic transcripts, their expression in the mutant cells follows the trend of annotated mRNAs (Fig. 4B,C). The reduction is consistently observed across gene expression levels (Fig. 4C). *Chd1*$^{-/-}$ ESCs have similar viability and cell cycle stage distribution than controls (supplementary material Fig. S3C), and show no upregulation of differentiation genes, indicating that the reduced RNA output per cell is not due to changes in cell state. Of note, this global shift in transcriptional output would be largely masked if the standard normalization for RNA amount, rather than cell number, had been carried out, explaining our initial confounding results with microarrays.

In order to validate the RNA-seq data, we carried out cell number-normalized qRT-PCR on independent samples for a group of genes covering a range of expression levels. In agreement with the RNA-seq data, every mRNA examined was found to be expressed at lower levels in *Chd1*$^{-/-}$ ESCs (supplementary material Fig. S7). This includes markers associated with pluripotency, such as *Oct4*, *Nanog* and *Klf2*, and several highly expressed genes associated with ribosome biogenesis and translation, such as *Rpl3*, *Rps9*, *Taf1d* and *Elf4a2*. Furthermore, the gene downregulation in *Chd1*$^{-/-}$ ESCs is already evident at primary mRNAs, prior to splicing (pre-mRNA, supplementary material Fig. S7A), suggesting that these defects are not due to altered splicing efficiency or mRNA stability but rather to a defect in RNAP II activity. In agreement with the recent results of Skene et al. in mouse embryonic fibroblasts (MEFs) (Skene et al., 2014), we observed that RNAP II S2p is also reduced in *Chd1*$^{-/-}$ ESCs in the gene body (GB) at a set of highly expressed genes tested using ChIP-qPCR (Fig. 4D), including *Gapdh*, *Klf2*, *Rpl3*, *Rpl9* and

Development (2015) 142, 118-127 doi:10.1242/dev.114843

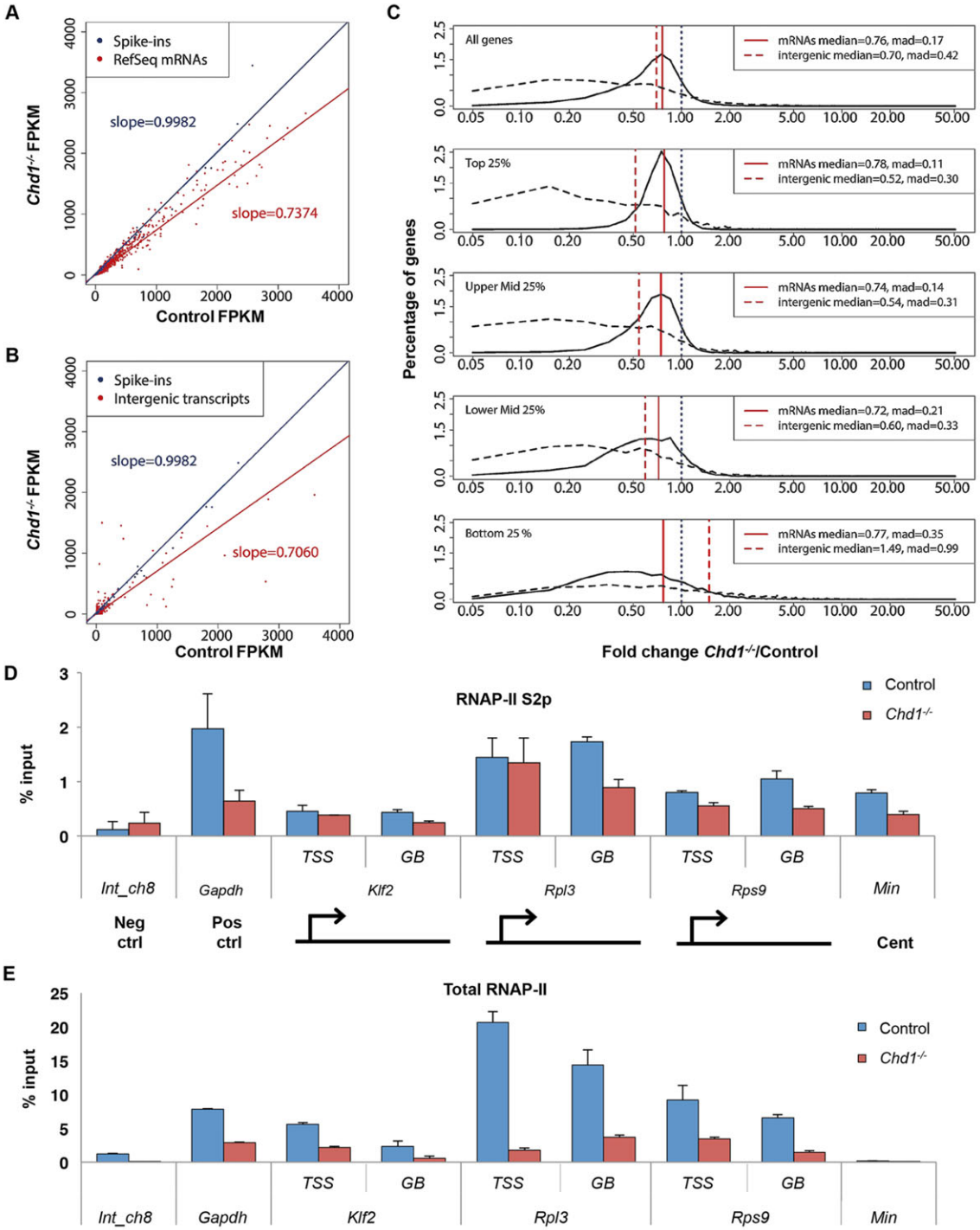

Fig. 4. Chd1 is required for optimal transcriptional output. (A,B) The cell number-normalized transcriptional output of *Chd1*$^{-/-}$ ESCs is reduced genome-wide at both known mRNAs (A) and intergenic transcripts (B). Blue dots and the blue regression line represent the exogenous spike-in RNAs used for RNA-seq data normalization, red dots and the red regression line represent known mRNA or intergenic transcripts levels in normalized FPKM. (C) The reduction in known mRNA and intergenic transcripts expression in *Chd1*$^{-/-}$ ESCs is observed across all expression levels. Shown are distribution plots of the fold change in mutant cells relative to controls using the RNA-seq data combined from both biological replicates for all genes or each quartile of gene expression levels. Vertical red unbroken lines mark the median fold change in mRNAs, vertical red dashed lines mark the median fold change in intergenic transcripts, vertical black dashed lines indicate the no change value (fold change=1). m.a.d., median absolute deviation. (D) RNAP II S2p levels are reduced in *Chd1*$^{-/-}$ cells, predominantly at the gene body (GB) of highly transcribed genes examined by ChIP-qPCR. (E) Total RNAP II is reduced at both the transcriptional start site (TSS) and GB in mutant ESCs. An intergenic region from chromosome 8 (Int_ch8) was used as negative control and the gene body of *Gapdh* as positive control. Min, minor satellites, corresponding to centromeric sequences. Data shown are representative of two (RNA-seq) or three (ChIP-qPCR) biological replicates.

minor satellite repeats, which are also transcribed by RNAP II (Lu and Gilbert, 2007). Interestingly, we found that total RNAP II is decreased at both the transcriptional start site (TSS) and GB in mutant ESCs (Fig. 4E). Taken together, these results suggest that Chd1 facilitates recruitment or retention of RNAP II to promote a globally elevated transcriptional output in ESCs.

Development (2015) 142, 118-127 doi:10.1242/dev.114843

Chd1 directly targets rDNA and regulates pre-rRNA transcription

The global role of Chd1 in RNAP II-mediated transcription led us to explore potential roles for Chd1 in ribosomal RNA (rRNA) transcription, which is carried out by RNAP I. Yeast Chd1 was previously found among several epigenetic factors that physically interact with ribosomal DNA (rDNA) (Hontz et al., 2009). ChIP-qPCR for Chd1-Flag, using the knock-in ES cell line (supplementary material Fig. S8), revealed a strong enrichment for Chd1 at the enhancer, promoter and gene body of rDNA, comparable to the levels observed at protein-coding genes (Fig. 5A). Moreover, cell number-normalized qRT-PCR using primers for nascent, pre-processed rRNA (pre-rRNA) showed a ~25% reduction upon Chd1 deletion (Fig. 5B). In agreement with these

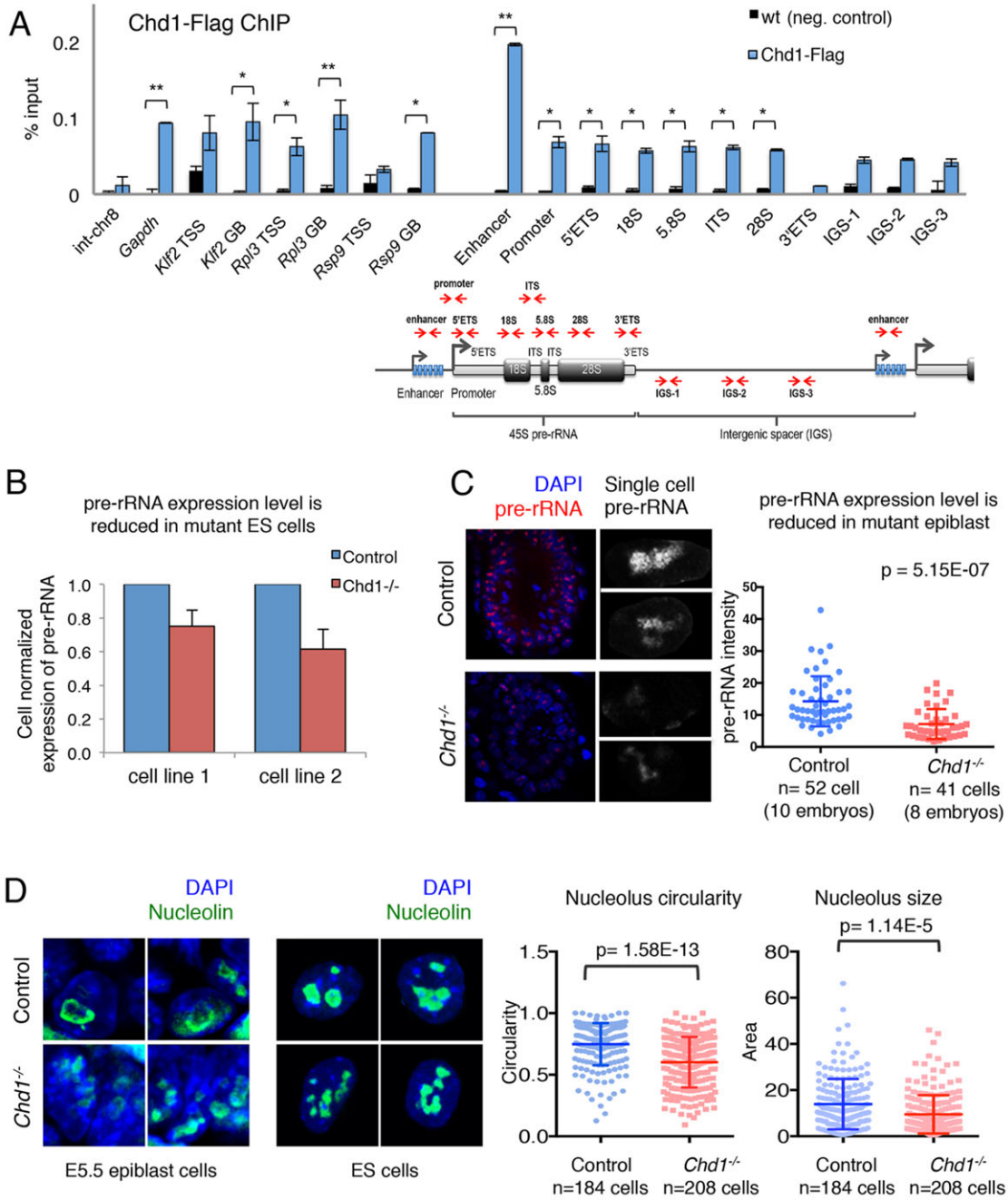

Fig. 5. Chd1 directly targets rDNA and regulates pre-rRNA transcription. (A) ChIP-qPCR shows *Chd1* enrichment at the enhancer, promoter and body of the rDNA transcription unit. A schematic representation of the ribosomal DNA repeat and primers used is shown below the graph. ETS, external transcribed spacer; ITS, internal transcribed spacer; IGS, intergenic spacer. Wild-type (WT) cells without the *Chd1-Flag* knock-in were used as negative control. Significance assessed using unpaired *t*-test, **P*<0.05, ***P*<0.01. (B) $Chd1^{-/-}$ ESCs express lower levels of pre-rRNA per cell. Cell number-normalized qRT-PCR was carried out in two independently derived ES cell lines. (C) $Chd1^{-/-}$ epiblast cells express lower levels of pre-rRNA per cell. Images are a reconstitution of four different planes of representative embryos processed for pre-rRNA FISH, with higher magnification images of representative single epiblast cells on the right. (D) IF for nucleolin in E5.5 epiblast cells *in vivo* and ESCs *in vitro* reveal that the nucleoli are more elongated and smaller in $Chd1^{-/-}$ cells than in control cells. Graphs represent quantification of this analysis of two independently derived ES cell lines. Circularity: control=0.75±0.17 and $Chd1^{-/-}$=0.60±0.21. 1.0 represents a perfect circle. Size: control=13.91±10.89 and $Chd1^{-/-}$=9.51±8.3. All results are mean±s.d.

Development (2015) 142, 118-127 doi:10.1242/dev.114843

findings in cultured ESCs, quantitative fluorescent *in situ* hybridization (FISH) (Raj et al., 2008) showed a significant reduction in pre-rRNA in mutant E5.5 epiblast cells *in vivo* (Fig. 5C). The RNA specificity of the pre-rRNA FISH was validated by loss of signal upon RNase I (but not DNase I) treatment in control embryos (supplementary material Fig. S9). Thus, Chd1 is required for the optimal output of rRNA both *in vitro* and *in vivo*.

Highly proliferative cells tend to have larger and rounder nucleoli, in which high levels of rRNA synthesis and ribosome assembly occur (Derenzini et al., 2000). Interestingly, we found that *Chd1*$^{-/-}$ cells, both in the E5.5 epiblast *in vivo* and in ESCs *in vitro*, have an altered nucleolar morphology, characterized by a decreased average size and circularity (Fig. 5D). These nucleolar abnormalities are observed throughout the mutant epiblast and in ESCs. Taken together, the data above indicate that Chd1 regulates the transcriptional output of rRNA, indirectly affecting nucleolar morphology of rapidly proliferating cells.

DISCUSSION

Our results indicate that a coordinately elevated global transcription by multiple RNAPs, regulated by factors such as Chd1, is essential for mouse embryonic development by sustaining the very rapid growth of the E5.5-6.5 epiblast (Snow, 1977). Data on the transcription factor cMyc lend some support to this model. cMyc directly promotes the activity of RNAP I, II and III (Oskarsson and Trumpp, 2005) and acts as a global amplifier of transcription (Lin et al., 2012; Nie et al., 2012). In mouse ESCs, the genome-wide location of Myc is highly correlated with H3K4me3, RNAP II and gene expression levels (Nie et al., 2012), very similar to that of Chd1 (Gaspar-Maia et al., 2009). In contrast to Chd1, however, *cMyc*$^{-/-}$ embryos have normal epiblast development and only arrest at mid-gestation (Davis et al., 1993), possibly due to redundancy with N-Myc (Mycn – Mouse Genome Informatics) and L-Myc (Mycl – Mouse Genome Informatics). Interestingly, mouse embryos mutant for Max, an obligate partner to Myc proteins, arrest in development at E5.5-6.5 (Shen-Li et al., 2000). Furthermore, *Chd1* RNAi was identified as synthetic lethal with cMyc overexpression in cultured human mammary epithelial cells (Kessler et al., 2012), indicating that Chd1 is required to support a Myc-driven hyper-proliferative state. In further support of this model, Chd1 directly interacts with Ssrp1 (Kelley et al., 1999), a component of the Facilitates chromatin transcription (FACT) complex, and *Srrp1*$^{-/-}$ embryos are capable of implanting but arrest by E5.5 (Cao et al., 2003). Moreover, increased transcriptional rates in the epiblast must not only be coordinated between different RNAPs, but they must also be intricately connected to regulation of the cell cycle. Indeed, there is evidence that ribosome biogenesis at the nucleolus, a process involving all three RNAPs, is a crucial sensor of cellular fitness that directly links transcriptional output to regulation of cell cycle progression (Kornberg, 1999; Rudra and Warner, 2004), something that deserves further exploration in the context of epiblast development.

ESCs exist in a state of hyper-transcription that correlates with a decondensed chromatin landscape (Efroni et al., 2008). Our data indicate that Chd1 is required to maintain this global hyper-transcription state. We note that a propensity for increased heterochromatin levels, initially reported in *Chd1* RNAi ESCs (Gaspar-Maia et al., 2009), can still be observed in *Chd1*$^{-/-}$ ESCs, as assessed by HP1a accumulation (supplementary material Fig. S6). This defect is less pronounced than that observed with RNAi, and appears to correlate with the growth rate deficit of the cells. Chd1 is associated with transcribed genes (Gaspar-Maia et al., 2009, and this study) and is depleted from heterochromatin (supplementary material Fig. S8C). Taken together, our results suggest that the primary role of Chd1 is to maintain high levels of RNAP I and II engagement in the transcribed proportion of the genome, including at protein-coding genes and rDNA, and this state of elevated transcription might in turn inhibit the formation or expansion of heterochromatin.

Our data show that Chd1 is not required for transcription per se, but rather potentiates it, and this role might be particularly crucial in very rapidly proliferating epiblast cells. A recent study on MEFs showed that Chd1 increases the turnover of promoter-proximal nucleosomes at expressed genes to facilitate release of RNAP II into productive elongation (Skene et al., 2014). That study also reported an increase in RNAP II paused at TSSs and a decrease in RNAP II elongating through GBs in MEFs transfected with a dominant-negative (DN) version of Chd1. In agreement with their work, we detect lower levels of elongating RNAP II at all GBs tested in *Chd1*$^{-/-}$ ESCs (Fig. 4). In contrast to the data of Skene and colleagues (Skene et al., 2014), we found significantly lower levels of total RNAP II at TSSs (Fig. 4E). Thus, in ESCs, Chd1 appears to promote recruitment or retention of RNAP II at the TSS, prior to elongation. The differences between the two studies might be due to the use of different approaches to inhibit Chd1 function: in our genetic deletion model, a functional Chd1 protein is not synthesized, whereas in the DN approach the full length protein is made, can still be recruited to promoters and bind H3K4me3, but is unable to remodel nucleosomes. This defect in nucleosome remodeling probably underlies the RNAP II elongation deficit described by Skene et al. (2014). Thus, it is possible that Chd1 regulates several steps of RNAP II engagement with transcription. The difference between the two studies might alternatively or additively be rooted in the difference in cell types, with RNAP II being more crucially dependent on Chd1 in rapidly growing pluripotent stem cells such as ESCs than in MEFs. The identification of proteins that interact with Chd1 in ESCs should help to elucidate further the biochemical regulation of the hyper-transcription state of pluripotent cells.

We had previously found Chd1 expression to be elevated in precursor cell populations, including somatic progenitor cells and the embryonic germline (Grskovic et al., 2007; Ramalho-Santos et al., 2002). It has recently been reported that the level of rRNA output regulates self-renewal versus differentiation in *Drosophila* germline stem cells (Zhang et al., 2014). Moreover, imbalances between constituents of the ribosome can lead to growth retardation, neural crest defects, anemia or cancer (Teng et al., 2013). It will be of interest to determine whether Chd1 regulates the transcriptional output of other expanding stem/progenitor cells during development as well as in cancer models.

MATERIALS AND METHODS

ESC targeting

A construct targeting exon 16 of *Chd1*, schematized in supplementary material Fig. S1A, was obtained from the knockout mouse project (KOMP, www.komp.org). This is a modular construct that allows for the generation of a mutant allele carrying a *lacZ* reporter driven by the endogenous *Chd1* promoter or a conditional (floxed) allele. The plasmid was linearized using AsiSI digestion and introduced into E14 ESCs by electroporation. Cells were selected using 250 µg/ml G418 (Sigma) and clones were identified based on *lacZ* expression and long-range PCR genotyping. To generate *Chd1*$^{-}$ or *Chd1*^{fl} alleles, pGK-NLS-Cre or pGK-FLPo plasmids, respectively, were introduced into targeted ESCs by electroporation. Clones were identified based on *lacZ* expression and PCR genotyping. Southern blotting was used

Development (2015) 142, 118-127 doi:10.1242/dev.114843

to confirm the correct integration and recombination of the construct (supplementary material Fig. S1B).

Generation of *Chd1* mutant mice

Correctly targeted and recombined ESCs were injected into C57BL/6 blastocysts and transferred to pseudo-pregnant females. Chimeras were crossed to C57BL/6 females and germline transmission was confirmed by PCR genotyping. $Chd1^{+/-}$ or $Chd1^{+/fl}$ mice were backcrossed in parallel to 129 and C57BL/6 strains. $Chd1^{+/-}$ were intercrossed to obtain $Chd1^{-/-}$ embryos. The *Sox2-Cre* line (Hayashi et al., 2002) was used to delete the floxed allele of *Chd1* specifically in the epiblast. The *ROSA26-CreER* line (Ventura et al., 2007) was used to delete the floxed allele of *Chd1* after derivation of ESCs (see below). Care and use of mice were in accordance with the guidelines of the University of California, San Francisco (UCSF) Institutional Animal Care and Use Committee (IACUC).

Embryo genotyping

Genomic DNA from embryos was extracted using the Extract-N-Amp Tissue PCR Kit (Sigma-Aldrich). Embryos were genotyped by PCR with the following primers: for the $Chd1^{-}$ allele, common forward 5′-ATTGCA-ATTTAGAGAGGACAG-3′, wild-type reverse 5′-GCCGGACACATAAC-CTGTCT-3′ and mutant reverse 5′-GGCAAGAACATAAAGTGACC-3′; for the $Chd1^{fl}$ allele, forward 5′-GCAATTTAGAGAGGACAGCGTGAC-TAAAGC-3′ and reverse 5′-ACCACGTACCAAGGCTTTCTGTAGTG-TAAT-3′.

β-galactosidase whole-mount staining

Embryos were fixed by 30 min on ice in 1% formaldehyde and 0.2% glutaraldehyde in X-gal buffer (5 mM EGTA, 2 mM $MgCl_2{\cdot}6H_2O$, 0.02% Triton X-100 and 0.01% deoxycholate in PBS) and then washed three times in X-gal buffer. Staining was carried out for 12-15 h at 37°C in staining solution [5 mM $K_3Fe(C_6FeK_3N_6)$, 5 mM $K_4Fe(C_6FeK_4N_6{\cdot}3H_2O)$, 0.5 mg/ml X-gal in X-gal buffer]. Finally, embryos were post-fixed in 4% paraformaldehyde for 60 min on ice and washed three times in PBS.

RNA WISH and IF

Standard WISH and IF protocols were used with minor modifications (Guzman-Ayala et al., 2004; Ralston & Rossant, 2008). Embryos were fixed in 4% paraformaldehyde in PBS overnight at 4°C. For WISH, embryos were dehydrated and rehydrated in a MeOH series before pre-hybridization for 20 min at 65°C and hybridization in the presence of 50-100 ng of digoxigenin (DIG)-labeled probes. Probes used for WISH were as described (Brennan et al., 2001). For IF, embryos or cells were permeabilized with 0.5% Triton X-100 for 20 min at room temperature and blocked in 0.5% BSA in PBS. Antibodies used for this study were: anti-Chd1 (Bethyl, A301-218A; 1:100 for ESC staining; and Santa Cruz, sc-49813; 1:50 for embryo staining); anti-Lefty1 (R&D, AF746; 1:50); anti-CENP-A (Cell Signaling, C51A7; 1:50); anti-Cleaved PARP (Cell Signaling, 95443; 1:100); anti-Flag (Sigma, F1804; 1:1000); anti-phospho-Histone H3 (Ser28) (Millipore, 07-145; 1:100). Embryos were imaged on a laser-scanning inverted confocal microscope (CTR 6500, Leica). *z*-stacks were taken at 5 µm intervals through the embryo, with each channel acquired sequentially. For nucleolar morphology analysis, E5.5 embryos or ESCs were stained for nucleolin (Abcam, 70493; 1:100) to demarcate the nucleolus. Nucleolar size (area) and shape (circularity) were measured using ImageJ (NIH). Unpaired *t*-test with Welch's correction was applied, assuming that the two data sets (control and mutants) being compared are independent and identically distributed (i.e. from different embryos but both normally distributed).

Pre-rRNA FISH

FISH was performed according to the manufacturer's instructions (Biosearch Technologies). Fixed embryos were permeabilized using 70% ethanol and hybridized at 37°C overnight with 1:250 of custom-made pre-rRNA Stellaris probes in RNA FISH hybridization beta buffer (Biosearch Technologies). Embryos were imaged using a 63× oil-immersion objective, every 0.5 µm, using the *z*-stack on a laser-scanning inverted confocal microscope (CTR 6500, Leica). Images were reconstituted and pre-RNA intensity for individual cells was quantified using ImageJ (NIH). For control experiments, embryos from wild-type crosses were treated for 15 min at 37°C in the presence of 100 units DNase I (BioLabs, M0303S) or 200 units of RNaseI (BioLabs, M0243S); then, the enzymes were deactivated by adding EDTA (5 mM final concentration) for 10 min at 70°C, followed by RNA FISH.

Epiblast cell number and EdU incorporation

The number of cells of the epiblast was scored using DAPI in four planes per embryo. Embryos were cultured in 40 µM EdU in a 1:1 mix of DMEM:fetal calf serum at 37°C, in 5% CO_2 for 15 min and then fixed in 4% paraformaldehyde in PBS overnight at 4°C. EdU detection was carried out according to the manufacturer's instructions using the Click-iT EdU Imaging Kit (Molecular Probes).

ESC derivation

ROSA26CreER;$Chd1^{fl/-}$ ESCs were derived in a medium described previously (Amano et al., 2009; Hayashi et al., 2002). In brief, E3.5 blastocysts were collected and transferred onto 12-well plates containing irradiated MEF feeder cells. ICM outgrowths were picked and dissociated in 0.05% trypsin-EDTA. Derived ES cell lines were plated on gelatin-coated plates to remove feeder cells and were genotyped. Independently derived lines of *ROSA26CreER;*$Chd1^{fl/-}$ ESCs were used for all *in vitro* analyses in this work, with the exception of the microarray studies and colony formation assays. These were carried out using $Chd1^{-/-}$ ESCs, derived by sequential targeting of $Chd1^{+/-}$ ESCs with the construct described above, and the Chd1-Flag ChIP-qPCR, which was carried out using a *Chd1* gene trap ES cell line (RRF067), in which a *Flag* epitope was knocked in at the *Chd1* locus by floxin technology (Singla et al., 2010).

Mouse cell culture

Mouse ESCs were routinely passaged in gelatin-coated six-well plates every other day. Cells counts were obtained using a Vi-CELL analyzer (Beckman Coulter) and either 200,000 or 600,000 cells were seeded per six-well well for serum/LIF or 2i/LIF media, respectively. Serum/LIF medium consists of 15% FBS, 1× penicillin/streptomycin, 1× non-essential amino acids, 0.057 mM β-mercaptoethanol and 1000 U/ml LIF (ESGro, Millipore) in high-glucose DMEM, supplemented with GlutaMAX and pyruvate (Gibco, 10569-10). 2i/LIF medium consists of 1× penicillin/streptomycin, 1× N2 supplement (Gibco, 17502048), 1× B27 supplement (Gibco, 17504-044), 50 µg/ml BSA Fraction V, 1000 U/ml LIF (ESGro, Millipore), 1 µM Mek inhibitor (PD0325901), and 3 µM Gsk3 inhibitor (CHIR99021) in a basal medium consisting of a 1:1 mix of DMEM-F12 (Gibco, 10565-018) and Neurobasal TM (Gibco, 21103049). *ROSA26CreER;*$Chd1^{fl/-}$ ESCs were control (EtOH)- or tamoxifen-treated (1 µM) for 48-72 h and then expanded without tamoxifen for 3-5 cell number-normalized passages in serum/LIF medium prior to further analyses (see below). Validation of *Chd1* deletion was carried out by qRT-PCR. Select control experiments were carried out using *ROSA26CreER;* $Chd1^{fl/+}$ ESCs. Epiblast-like cell differentiation was performed on a feeder layer of irradiated mouse embryonic fibroblasts essentially as described (Guo et al., 2009). The medium for differentiation of epiblast-like cells was the same as the 2i/LIF medium with the following changes: Lif, Mek inhibitor and Gsk3 inhibitor were removed; activin A (Inhba – Mouse Genome Informatics) (20 ng/ml) and Fgf2 (12 ng/ml) were added.

Western blotting

Two-color western blotting was performed according to the manufacturer's instructions (LiCor). Samples were prepared using standard RIPA buffer. The soluble fraction was isolated by centrifugation and loaded onto a denaturing gradient SDS acrylamide gel. Transfer to a PVDF membrane (Millipore) was accomplished at 30 V overnight at 4°C. Primary antibodies used were: anti-Chd1 (Santa Cruz, SC-49813; 1:1000); anti-TopoI (Top1 – Mouse Genome Informatics) (Abcam, ab85038; 1:1000); anti-Flag (Sigma, F1804; 1:1000). Two-color blots were false-colored to black and white using the manufacturer's software (LiCor).

Viability and cell cycle analyses in ESCs

Control and $Chd1^{-/-}$ ESCs derived from two independent lines of *ROSA26CreER;*$Chd1^{fl/-}$ ESCs were analyzed. Viability was calculated by

Development (2015) 142, 118-127 doi:10.1242/dev.114843

analysis of Trypan Blue exclusion with a Beckman Coulter Vi-CELL analyzer. Cell cycle analysis was performed by flow cytometry for EdU (S phase) and FxCycle Violet (DNA content) in an LSR II (BD Biosciences).

ChIP-qPCR

ChIP-qPCR was performed as described (Sachs et al., 2013), using 2-2.4 µg of antibody per IP. In the case of Chd1-Flag IP, 1×10^7 cells were used, and cells were crosslinked in 1% formaldehyde for 30 min. The following primary antibodies used were: anti-RNAP II S2p (Abcam, ab5095); anti-total RNAP II (Diagenode, C15200004); anti-Flag (Sigma, F1804); anti-rabbit IgG (Abcam, ab46540). Quantification was performed using the KAPA SYBR FAST qPCR kit (KK4604) on an ABI 7900HT device. Primers used are listed in supplementary material Table S1.

Cell number-normalized RNA-seq

Two independently derived lines of *ROSA26CreER;Chd1*$^{fl/-}$ ESCs were either control-(EtOH) or tamoxifen-treated as described above. Cells were counted twice at different dilutions on a Vi-CELL analyzer and total RNA was isolated from equal numbers of viable cells. RNA was isolated using the RNeasy kit (QIAGEN) with on-column DNase I digestion. Total RNA was quantified using a Qubit fluorometer (Invitrogen). Equal elution volumes of RNA corresponding to ∼1 µg of total RNA were mixed with 1 µl of a 1:10 dilution of Mix#1 External RNA Controls Consortium (ERCC) RNA spike-in controls, containing 92 polyadenylated transcripts over a range of concentrations (Life Technologies, 4456740). rRNA depletion was performed using the Ribo-Zero rRNA removal kit (Epicentre, MRZH116). Strand-specific libraries were generated using the Illumina TruSeq Stranded mRNA kit (RS-122-2101). Libraries were prepared using barcoded adaptors, pooled and sequenced over two lanes of an Illumina HiSeq 2500 in rapid mode for paired-end reads of 100 bases at the UC Davis Genome Center. RNA-Seq reads were first trimmed of Illumina adapter sequence. Any pairs with reads containing less than 40 bases of insert sequence were discarded. The remaining trimmed reads were aligned by TopHat (v2.0.10) with a custom genome containing the mm9 mouse assembly, with the ERCC spike-in sequences added. The TopHat alignment was guided by a custom reference gene set, consisting of RefSeq genes >150 bases (downloaded 30 December 2013 from the UCSC Genome Browser, http://genome.ucsc.edu/, mm9) as well as the ERCC spike-in sequences. Only properly paired reads mapping uniquely to the combined mm9+ERCC genome were retained for further analysis. To obtain raw fragments per kilobase of transcript per million mapped reads (FPKM) values in the paired mutant and control libraries, reads were first processed through Cufflinks (v2.2.0), using the custom gene set as a guide but allowing assembly of novel transcripts. Throughout the mapping and quantification procedures, the 'fr-secondstrand' option was invoked whenever possible to indicate the strand-specificity of the sequencing libraries. The custom reference genome was also given to Cufflinks and Cuffdiff for bias correction, and the '–max-bundle-frags' option was set to 100,000,000 to enable quantification of highly expressed transcripts. Local regression (loess) normalization of the paired mutant and control FPKM values obtained from Cuffdiff was performed as described previously (Lovén et al., 2012). The loess-normalized FPKM values were used in all subsequent analyses. For the fold change distribution plots, only genes with expression of at least 0.1 FPKM in the control sample were considered for each pair. Data have been deposited in GEO (accession number: GSE57609).

Cell number-normalized qRT-PCR

Total RNA from equal numbers of cells from two independently derived lines of *ROSA26CreER;Chd1*$^{fl/-}$ ESCs treated with either control (EtOH) or tamoxifen was isolated as described above. Equal elution volumes of RNA were used to generate cDNA using the High-Capacity cDNA Reverse Transcription Kit (Life Technologies, 4368814). Quantification was performed using the KAPA SYBR FAST qPCR kit (KK4604) on an ABI 7900HT instrument. The $2^{-\Delta\Delta CT}$ method (Applied Biosystems) was used to calculate the expression level of each gene in mutant cells relative to the level in matched control cells, which was set as 1. Primers used are listed in supplementary material Table S2.

Acknowledgements

We thank Davide Ruggero, Barbara Panning, Alexandre Gaspar-Maia, Robert Blelloch, Diana Laird, Marco Conti and members of the Santos laboratory for helpful discussions and critical reading of the manuscript. We are grateful to Minh To for technical assistance with Southern blotting, Daniel B. Constam for *in situ* probes, Laure Blouin for technical assistance with WISH, Camilo Guzman for advice with statistical analysis, and Julie Hunkapiller and Jeremy Reiter for advice with floxin technology.

Competing interests

The authors declare no competing financial interests.

Author contributions

M.R.-S. directed the project. M.G.-A. performed all of the experiments in embryos, with technical assistance from P.W. M.G.-A. also analyzed heterochromatin levels and nucleolar structure in ESCs. M.S. carried out analyses of self-renewal, differentiation, transcriptional output and S2p RNAP in ESCs. He also developed the Chd1-Flag ESCs, with assistance from R.N. F.M.K. carried out gene targeting, Southern blotting and cell cycle analyses in ESCs. C.O. analyzed the RNA-seq data with aid and supervision from J.S.S. and M.R.-S. A.B.-K. performed Chd1-Flag and total RNAP II ChIP. C.-J.L. and M.S. derived and genotyped ESCs. P.W., F.M.K. and M.G.-A. managed the mouse colony. P.W. contributed to the culture of ESCs under the supervision of M.G.-A. and M.S. M.G.-A., M.S. and M.R.-S. designed experiments, interpreted the results and wrote the manuscript. M.G.-A. led the revisions of the manuscript.

Funding

M.G.-A. was partially supported by a T32 grant from the National Institutes of Health (NIH) to the UCSF Center for Reproductive Sciences. F.M.K. was supported by the Agency for Science, Technology and Research (Singapore). R.N. was supported by the SFSU CIRM bridges program. This work was supported by NIH grant U54HD055764, by a Sontag Foundation Distinguished Scientist Award to J.S.S. and by NIH New Innovator Award DP2OD004698 to M.R.-S. Deposited in PMC for release after 12 months.

Supplementary material

Supplementary material available online at
http://dev.biologists.org/lookup/suppl/doi:10.1242/dev.114843/-/DC1

References

Ahmed, K., Dehghani, H., Rugg-Gunn, P., Fussner, E., Rossant, J. and Bazett-Jones, D. P. (2010). Global chromatin architecture reflects pluripotency and lineage commitment in the early mouse embryo. *PLoS ONE* **5**, e10531.

Amano, T., Papanikolaou, T., Sung, L.-Y., Lennington, J., Conover, J. and Yang, X. (2009). Nuclear transfer embryonic stem cells provide an in vitro culture model for Parkinson's disease. *Cloning Stem Cells* **11**, 77-88.

Ang, Y.-S., Tsai, S.-Y., Lee, D.-F., Monk, J., Su, J., Ratnakumar, K., Ding, J., Ge, Y., Darr, H., Chang, B. et al. (2011). Wdr5 mediates self-renewal and reprogramming via the embryonic stem cell core transcriptional network. *Cell* **145**, 183-197.

Bedzhov, I. and Zernicka-Goetz, M. (2014). Self-organizing properties of mouse pluripotent cells initiate morphogenesis upon implantation. *Cell* **156**, 1032-1044.

Brennan, J., Lu, C. C., Norris, D. P., Rodriguez, T. A., Beddington, R. S. P. and Robertson, E. J. (2001). Nodal signalling in the epiblast patterns the early mouse embryo. *Nature* **411**, 965-969.

Cao, S., Bendall, H., Hicks, G. G., Nashabi, A., Sakano, H., Shinkai, Y., Gariglio, M., Oltz, E. M. and Ruley, H. E. (2003). The high-mobility-group box protein SSRP1/T160 is essential for cell viability in day 3.5 mouse embryos. *Mol. Cell. Biol.* **23**, 5301-5307.

Davis, A. C., Wims, M., Spotts, G. D., Hann, S. R. and Bradley, A. (1993). A null c-myc mutation causes lethality before 10.5 days of gestation in homozygotes and reduced fertility in heterozygous female mice. *Genes Dev.* **7**, 671-682.

Derenzini, M., Trerè, D., Pession, A., Govoni, M., Sirri, V. and Chieco, P. (2000). Nucleolar size indicates the rapidity of cell proliferation in cancer tissues. *J. Pathol.* **191**, 181-186.

Efroni, S., Duttagupta, R., Cheng, J., Dehghani, H., Hoeppner, D. J., Dash, C., Bazett-Jones, D. P., Le Grice, S., McKay, R. D. G., Buetow, K. H. et al. (2008). Global transcription in pluripotent embryonic stem cells. *Cell Stem Cell* **2**, 437-447.

Flanagan, J. F., Mi, L.-Z., Chruszcz, M., Cymborowski, M., Clines, K. L., Kim, Y., Minor, W., Rastinejad, F. and Khorasanizadeh, S. (2005). Double chromodomains cooperate to recognize the methylated histone H3 tail. *Nature* **438**, 1181-1185.

Flaus, A., Martin, D. M. A., Barton, G. J. and Owen-Hughes, T. (2006). Identification of multiple distinct Snf2 subfamilies with conserved structural motifs. *Nucleic Acids Res.* **34**, 2887-2905.

Gaspar-Maia, A., Alajem, A., Polesso, F., Sridharan, R., Mason, M. J., Heidersbach, A., Ramalho-Santos, J., McManus, M. T., Plath, K., Meshorer,

E. et al. (2009). Chd1 regulates open chromatin and pluripotency of embryonic stem cells. *Nature* **460**, 863-868.
Gkikopoulos, T., Schofield, P., Singh, V., Pinskaya, M., Mellor, J., Smolle, M., Workman, J. L., Barton, G. J. and Owen-Hughes, T. (2011). A role for Snf2-related nucleosome-spacing enzymes in genome-wide nucleosome organization. *Science* **333**, 1758-1760.
Grskovic, M., Chaivorapol, C., Gaspar-Maia, A., Li, H. and Ramalho-Santos, M. (2007). Systematic identification of cis-regulatory sequences active in mouse and human embryonic stem cells. *PLoS Genet.* **3**, e145.
Guo, G., Yang, J., Nichols, J., Hall, J. S., Eyres, I., Mansfield, W. and Smith, A. (2009). Klf4 reverts developmentally programmed restriction of ground state pluripotency. *Development* **136**, 1063-1069.
Guzman-Ayala, M., Ben-Haim, N., Beck, S. and Constam, D. B. (2004). Nodal protein processing and fibroblast growth factor 4 synergize to maintain a trophoblast stem cell microenvironment. *Proc. Natl. Acad. Sci. USA* **101**, 15656-15660.
Hayashi, S., Lewis, P., Pevny, L. and McMahon, A. P. (2002). Efficient gene modulation in mouse epiblast using a Sox2Cre transgenic mouse strain. *Mech. Dev.* **119** Suppl. 1, S97-S101.
Hébert, J. M., Boyle, M. and Martin, G. R. (1991). mRNA localization studies suggest that murine FGF-5 plays a role in gastrulation. *Development* **112**, 407-415.
Hennig, B. P., Bendrin, K., Zhou, Y. and Fischer, T. (2012). Chd1 chromatin remodelers maintain nucleosome organization and repress cryptic transcription. *EMBO Rep.* **13**, 997-1003.
Hontz, R. D., Niederer, R. O., Johnson, J. M. and Smith, J. S. (2009). Genetic identification of factors that modulate ribosomal DNA transcription in Saccharomyces cerevisiae. *Genetics* **182**, 105-119.
Jansen, L. E. T., Black, B. E., Foltz, D. R. and Cleveland, D. W. (2007). Propagation of centromeric chromatin requires exit from mitosis. *J. Cell Biol.* **176**, 795-805.
Kelley, D. E., Stokes, D. G. and Perry, R. P. (1999). CHD1 interacts with SSRP1 and depends on both its chromodomain and its ATPase/helicase-like domain for proper association with chromatin. *Chromosoma* **108**, 10-25.
Kessler, J. D., Kahle, K. T., Sun, T., Meerbrey, K. L., Schlabach, M. R., Schmitt, E. M., Skinner, S. O., Xu, Q., Li, M. Z., Hartman, Z. C. et al. (2012). A SUMOylation-dependent transcriptional subprogram is required for Myc-driven tumorigenesis. *Science* **335**, 348-353.
Konev, A. Y., Tribus, M., Park, S. Y., Podhraski, V., Lim, C. Y., Emelyanov, A. V., Vershilova, E., Pirrotta, V., Kadonaga, J. T., Lusser, A. et al. (2007). CHD1 motor protein is required for deposition of histone variant H3.3 into chromatin in vivo. *Science* **317**, 1087-1090.
Kornberg, R. D. (1999). Eukaryotic transcriptional control. *Trends Cell Biol.* **9**, M46-M49.
Lewis, N. E. and Rossant, J. (1982). Mechanism of size regulation in mouse embryo aggregates. *J. Embryol. Exp. Morphol.* **72**, 169-181.
Lin, J. J., Lehmann, L. W., Bonora, G., Sridharan, R., Vashisht, A. A., Tran, N., Plath, K., Wohlschlegel, J. A. and Carey, M. (2011). Mediator coordinates PIC assembly with recruitment of CHD1. *Genes Dev.* **25**, 2198-2209.
Lin, C. Y., Lovén, J., Rahl, P. B., Paranal, R. M., Burge, C. B., Bradner, J. E., Lee, T. I. and Young, R. A. (2012). Transcriptional amplification in tumor cells with elevated c-Myc. *Cell* **151**, 56-67.
Liu, P., Wakamiya, M., Shea, M. J., Albrecht, U., Behringer, R. R. and Bradley, A. (1999). Requirement for Wnt3 in vertebrate axis formation. *Nat. Genet.* **22**, 361-365.
Lovén, J., Orlando, D. A., Sigova, A. A., Lin, C. Y., Rahl, P. B., Burge, C. B., Levens, D. L., Lee, T. I. and Young, R. A. (2012). Revisiting global gene expression analysis. *Cell* **151**, 476-482.
Lu, J. and Gilbert, D. M. (2007). Proliferation-dependent and cell cycle regulated transcription of mouse pericentric heterochromatin. *J. Cell Biol.* **179**, 411-421.
McDaniel, I. E., Lee, J. M., Berger, M. S., Hanagami, C. K. and Armstrong, J. A. (2008). Investigations of CHD1 function in transcription and development of Drosophila melanogaster. *Genetics* **178**, 583-587.
Meshorer, E. and Misteli, T. (2006). Chromatin in pluripotent embryonic stem cells and differentiation. *Nat. Rev. Mol. Cell. Biol.* **7**, 540-546.
Mesnard, D., Guzman-Ayala, M. and Constam, D. B. (2006). Nodal specifies embryonic visceral endoderm and sustains pluripotent cells in the epiblast before overt axial patterning. *Development* **133**, 2497-2505.
Nie, Z., Hu, G., Wei, G., Cui, K., Yamane, A., Resch, W., Wang, R., Green, D. R., Tessarollo, L., Casellas, R. et al. (2012). c-Myc is a universal amplifier of expressed genes in lymphocytes and embryonic stem cells. *Cell* **151**, 68-79.
Okada, M., Okawa, K., Isobe, T. and Fukagawa, T. (2009). CENP-H-containing complex facilitates centromere deposition of CENP-A in cooperation with FACT and CHD1. *Mol. Biol. Cell* **20**, 3986-3995.
Oskarsson, T. and Trumpp, A. (2005). The Myc trilogy: lord of RNA polymerases. *Nat. Cell Biol.* **7**, 215-217.
Perea-Gomez, A., Vella, F. D. J., Shawlot, W., Oulad-Abdelghani, M., Chazaud, C., Meno, C., Pfister, V., Chen, L., Robertson, E., Hamada, H. et al. (2002). Nodal antagonists in the anterior visceral endoderm prevent the formation of multiple primitive streaks. *Dev. Cell* **3**, 745-756.
Pointner, J., Persson, J., Prasad, P., Norman-Axelsson, U., Strålfors, A., Khorosjutina, O., Krietenstein, N., Svensson, J. P., Ekwall, K. and Korber, P. (2012). CHD1 remodelers regulate nucleosome spacing in vitro and align nucleosomal arrays over gene coding regions in S. pombe. *EMBO J.* **31**, 4388-4403.
Power, M.-A. and Tam, P. P. L. (1993). Onset of gastrulation, morphogenesis and somitogenesis in mouse embryos displaying compensatory growth. *Anat. Embryol.* **187**, 493-504.
Raj, A., van den Bogaard, P., Rifkin, S. A., van Oudenaarden, A. and Tyagi, S. (2008). Imaging individual mRNA molecules using multiple singly labeled probes. *Nat. Methods* **5**, 877-879.
Ralston, A. and Rossant, J. (2008). Cdx2 acts downstream of cell polarization to cell-autonomously promote trophectoderm fate in the early mouse embryo. *Dev. Biol.* **15**, 614-629.
Ramalho-Santos, M., Yoon, S., Matsuzaki, Y., Mulligan, R. C. and Melton, D. A. (2002). "Stemness": transcriptional profiling of embryonic and adult stem cells. *Science* **298**, 597-600.
Rosner, M. H., Vigano, M. A., Ozato, K., Timmons, P. M., Poirie, F., Rigby, P. W. J. and Staudt, L. M. (1990). A POU-domain transcription factor in early stem cells and germ cells of the mammalian embryo. *Nature* **345**, 686-692.
Rudra, D. and Warner, J. R. (2004). What better measure than ribosome synthesis? *Genes Dev.* **18**, 2431-2436.
Sachs, M., Onodera, C., Blaschke, K., Ebata, K. T., Song, J. S. and Ramalho-Santos, M. (2013). Bivalent chromatin marks developmental regulatory genes in the mouse embryonic germline in vivo. *Cell Rep.* **3**, 1777-1784.
Shen-Li, H., O'Hagan, R. C., Hou, H., Horner, J. W., Lee, H. W. and DePinho, R. A. (2000). Essential role for Max in early embryonic growth and development. *Genes Dev.* **14**, 17-22.
Sims, R. J., Chen, C.-F., Santos-Rosa, H., Kouzarides, T., Patel, S. S. and Reinberg, D. (2005). Human but not yeast CHD1 binds directly and selectively to histone H3 methylated at lysine 4 via its tandem chromodomains. *J. Biol. Chem.* **280**, 41789-41792.
Sims, R. J., Millhouse, S., Chen, C.-F., Lewis, B. A., Erdjument-Bromage, H., Tempst, P., Manley, J. L. and Reinberg, D. (2007). Recognition of trimethylated histone H3 lysine 4 facilitates the recruitment of transcription postinitiation factors and pre-mRNA splicing. *Mol. Cell* **28**, 665-676.
Singla, V., Hunkapiller, J., Santos, N., Seol, A. D., Norman, A. R., Wakenight, P., Skarnes, W. C. and Reiter, J. F. (2010). Floxin, a resource for genetically engineering mouse ESCs. *Nat. Methods* **7**, 50-52.
Skene, P. J., Hernandez, A. E., Groudine, M. and Henikoff, S. (2014). The nucleosomal barrier to promoter escape by RNA polymerase II is overcome by the chromatin remodeler Chd1. *Elife* **3**, e02042.
Snider, A. C., Leong, D., Wang, Q. T., Wysocka, J., Yao, M. W. M. and Scott, M. P. (2013). The chromatin remodeling factor Chd1l is required in the preimplantation embryo. *Biol. Open* **2**, 121-131.
Snow, M. (1977). Gastrulation in the mouse: growth and regionalization of the epiblast. *Development* **42**, 293-303.
Stokes, D. G., Tartof, K. D. and Perry, R. P. (1996). CHD1 is concentrated in interbands and puffed regions of Drosophila polytene chromosomes. *Proc. Natl. Acad. Sci. USA* **93**, 7137-7142.
Teng, T., Thomas, G. and Mercer, C. A. (2013). Growth control and ribosomopathies. *Curr. Opin. Genet. Dev.* **23**, 63-71.
Tsukiyama, T., Palmer, J., Landel, C. C., Shiloach, J. and Wu, C. (1999). Characterization of the imitation switch subfamily of ATP-dependent chromatin-remodeling factors in Saccharomyces cerevisiae. *Genes Dev.* **13**, 686-697.
Ventura, A., Kirsch, D. G., McLaughlin, M. E., Tuveson, D. A., Grimm, J., Lintault, L., Newman, J., Reczek, E. E., Weissleder, R. and Jacks, T. (2007). Restoration of p53 function leads to tumour regression in vivo. *Nature* **445**, 661-665.
Woodage, T., Basrai, M. A., Baxevanis, A. D., Hieter, P. and Collins, F. S. (1997). Characterization of the CHD family of proteins. *Proc. Natl. Acad. Sci. USA* **94**, 11472-11477.
Zhang, Q., Shalaby, N. A. and Buszczak, M. (2014). Changes in rRNA transcription influence proliferation and cell fate within a stem cell lineage. *Science* **343**, 298-301.